Research Article | Vol. 31, No. 21 / 9 Oct 2023 / Optics Express 33842
Optics EXPRESS

Enhanced measurement of tiny rotational angles using conjugate orbital angular momentum modes

DAN WEI,[1] LUYI WANG,[2] JIANTAO MA,[2] LIN HE,[1] YONG ZHANG,[2,*] MIN XIAO,[2,3] AND YONGQING LI[1,4,5]

[1]School of Electronic Engineering & Intelligentization, Dongguan University of Technology, Dongguan, Guangdong 523808, China
[2]National Laboratory of Solid State Microstructures, College of Engineering and Applied Sciences, and School of Physics, Nanjing University, Nanjing 210093, China
[3]Department of Physics, University of Arkansas, Fayetteville, Arkansas 72701, USA
[4]Department of Physics, East Carolina University, Greenville, North Carolina 27858-4353, USA
[5]liy@ecu.edu
*zhangyong@nju.edu.cn

Abstract: We report the enhanced experimental measurement of tiny rotational angles using two conjugate OAM modes upon rotation of a Dove prism. The two conjugate OAM modes interfere in a petal-like pattern and the orientation of the pattern depends on the phase difference between the two modes. We propose an accurate method of digital image processing to measure the tiny rotational angles of the Dove prism. In the presence of an imperfect pattern and light path, the measurement precision was enhanced by a factor of l. This scheme has potential applications in high-precision sensing and monitoring of tiny rotation angles.

1. Introduction

In 1992, Allen reported that a photon in a light beam comprising an azimuthal phase term, $\exp(il\theta)$, carries an orbital angular momentum (OAM) of $l\hbar$ [1]. In contrast with spin angular momentum, which has only two possible values of $\pm\hbar$, the theoretically unlimited values of l, in principle, provide an infinite range of achievable OAM states. This gives OAM an important degree of freedom in both the classical and quantum information domains [2–5]. Using classical coherent states, the OAM of light can be applied in communications to increase system capacities and spectral efficiencies [6,7]. When combined with quantum characteristics, OAM light beams with different values of the mode index, l, can produce high-dimensional entanglement to provide increased security and robustness and high information capacities for quantum communications [8,9]. These application requirements have stimulated the development of high-order OAM generation methods. Earlier methods have used holographic diffraction gratings [10], Q-plates [11,12] and spiral phase plates [13], whereas newer methods are based on optical fibers [14], integrated vortex emitters [15–17], lasers [18,19], and nonlinear optics techniques [20–24].

In addition to providing high-order states, OAM modes feature a vortex wavefront. These two characteristics enable the application of OAM modes in precise detection, such as measuring speeds [25–28], rotational symmetry [29], and OAM spectra [30,31] and angles [32–37]. A Mach–Zehnder interferometer is normally used to detect the phase induced by rotation of the OAM mode [38]. As an alternative scheme, a Sagnac interferometer can double the signal and thus improve the measurement accuracy [39]. However, because of environmental noise, the interferometer requires plenty of additional optical and electronic devices to maintain high interference contrast and steady phase difference between its two arms.

Our scheme amplifies tiny rotational angles by l using the geometric phase distribution of the OAM. The rotation of the spatial intensity distribution of two conjugate OAM modes depends

#498392 https://doi.org/10.1364/OE.498392
Journal © 2023 Received 20 Jun 2023; revised 5 Aug 2023; accepted 30 Aug 2023; published 25 Sep 2023

Optics EXPRESS

on the phase difference between the two modes. Instead of using an interferometer, digital image processing is proposed to measure the phase variation introduced by a rotating Dove prism. OAM-enhanced measurement is demonstrated in the presence of defects in both the spots and light paths. The above advantages make the proposed method more practical that existing methods.

We consider that an OAM light beam with $+l$ and $-l$ conjugate OAM modes passes through a Dove prism oriented at an angle of φ, where the Dove prism is an optical element that rotates the incident beam by 2φ [40]. If the Dove prism rotates by a small angle, our objective is to find an effective way to measure it.

2. Theory

A Laguerre–Gaussian (LG) beam is a typical OAM mode with azimuthal and radial indices l and p, which can be written in cylindrical coordinates as

$$LG_{lp}(r,\theta) = A_{pl}(-i)^{2p+l+1}\left(\sqrt{2}r/\omega\right)^{|l|}L_p^{|l|}(2r^2/\omega)\exp(il\theta), \tag{1}$$

where $\exp(il\theta)$ is the azimuthal phase dependence, A_{pl} is a normalized constant, ω is the beam waist, and $L_p^{|l|}(\cdot)$ is the generalized Laguerre polynomial. Equation (1) can be re-written as:

$$E_l(r,\theta) = R_{lp}(r)\exp(il\theta), \tag{2}$$

where $R_{lp}(r)$ describes the radial intensity dependence of the field of Eq. (1). It was previously recognized that each photon within such a LG beam carries a well-defined OAM of $l\hbar$ [1]. The expression of a $-l$ LG beam only includes a minus sign in the "θ" dependence of Eq. (2), in contrast with the l LG beam. When the Dove prism is oriented at an angle of φ, the expression of the total field of the output beam (i.e., a combination of the two $+l$ and $-l$ conjugate LG beams) becomes

$$\begin{aligned} &E_l(r,\theta) + E_{-l}(r,\theta) \\ &= R_{lp}(r)\exp[il(\theta-2\varphi)] + R_{lp}(r)\exp[-il(\theta-2\varphi)] \\ &= 2R_{lp}(r)\cos[l(\theta-2\varphi)]. \end{aligned} \tag{3}$$

This implies a rotation of the electric field with an angle of 2φ. The light intensity $I(r,\theta)$ of the output beam is

$$I(r,\theta) = 2|R_{lp}(r)|^2[1+\cos 2l(\theta-2\varphi)] \tag{4}$$

Thus, there is an angular modulation of the intensity of the output field. Figure 1 shows the petal-like patterns according to Eq. (4), where the number of petals is twice the azimuthal index of the beam ($2\,l$). 2φ is the rotation angle of the pattern, and the direction of arrow represents the origin of the azimuthal angle, θ. It should be noted that the origin of the azimuthal angle must be chosen along the direction of one intensity maximum of the pattern before rotating the Dove prism. Figure 1(a–c) correspond to the normalized simulated intensities for $l = 1, 2, 3$, respectively.

To measure φ, the intensity of the petal-like pattern $I(r,\theta)$ is divided into $4\,l$ regions from the zero azimuthal angle evenly (see Fig. 1). The total intensity of the n-th region is:

$$\begin{aligned} I_l(n) &= \int_0^{\infty} r \int_{(n-1)\pi/2l}^{n\pi/2l} 2|R_{lp}(r)|^2[1+\cos(2l\theta-4l\varphi)]d\theta dr dr \\ &= \int_0^{\infty} |R_{lp}(r)|^2 r dr\left[\tfrac{\pi}{l} - (-1)^n\tfrac{2}{l}\sin(4l\varphi)\right] \end{aligned} \tag{5}$$

Optics EXPRESS

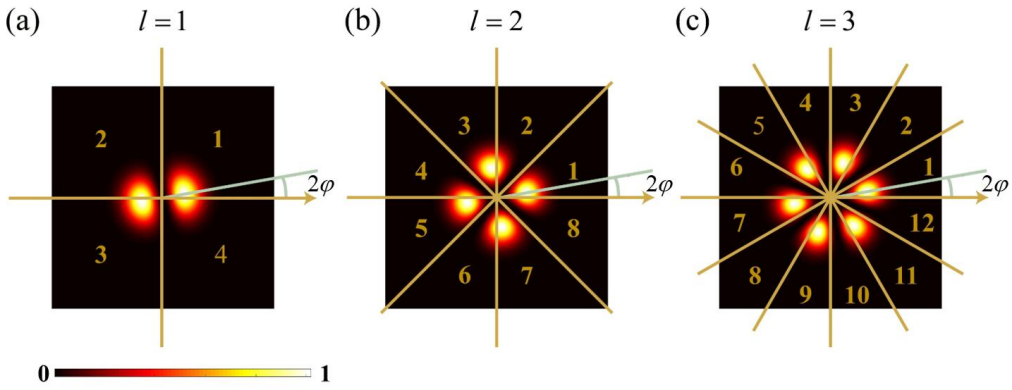

Fig. 1. Normalized petal-like pattern of the intensity of an OAM beam passing through a Dove prism, with (a), (b), and (c) corresponding to $l = 1, 2, 3$, respectively. The superposition of the l and $-l$ conjugate beams ($l = 1, 2, 3$) leads to interference patterns in which the number of petals is twice the topological charge, l. The patterns are divided into $4\,l$ (4, 8, 12) regions from the zero azimuthal angle. The direction of the arrow represents the origin of the azimuthal angle, θ. 2φ is the rotation angle of the pattern when the Dove prism rotates by an angle of φ.

with $n \in [1, 2 \ldots 4l]$. When the intensity of the adjacent region is subtracted, the total differential intensity S_l, is:

$$S_l = I_l(1) - I_l(2) + \cdots - I_l(4l) = P \sin(4l\varphi) \tag{6}$$

where $P = 8 \int_0^\infty |R_{lp}(r)|^2 r dr$ is the amplitude of S_l, which depends on the total intensity of the pattern. When φ is sufficiently small, S_l satisfies

$$S_l \sim 4Pl\varphi \tag{7}$$

Thus, S_l is proportional to tiny φ. The ratio of S_l to φ has a linear relationship with l and P, which enables the sensitive measurement of tiny rotational angle from the rotational pattern.

3. Experimental configuration and results

The experimental configuration to probe the tiny rotation of the Dove prism is sketched in Fig. 2(a). The laser used is a continuous-wave diode-pumped solid-state laser (Mephisto MOPA 25W) operating at 1064 nm with an ultra-narrow linewidth. The fundamental mode of the laser is transformed into $\pm l$ OAM modes using an SLM (Meadowlark Optics, BDM512-1064). We prepared phase patterns (Fig. 2(b)) and displayed them in the SLM. In Fig. 2(b), the top, middle, and bottom patterns are used to produce OAM beams with $+l$ and $-l$ conjugate OAM modes corresponding to $l = 2$, 20, 40, respectively. The OAM beam passes through the Dove prism and then the output intensity is recorded by the CCD (Newport, LBP2).

The results are shown in Fig. 3(a) ($l = 20$) and 3(b) ($l = 40$), in which the left and the right sides are the simulated and experimental patterns, respectively. The experimental patterns are imperfect, in contrast with the simulated patterns, probably because of a defective SLM pattern display. There is a large amount of stray light in the central and marginal regions of the experimental patterns, especially for the high-order pattern. The fields of the high-order patterns show finer phase distribution and more obvious divergence. These qualities are limited by the resolution of the SLM and the aperture of the optical device. Thus, the effect of the imperfect experimental pattern on the measurement needs to be further investigated. Here, we selected the

Optics EXPRESS

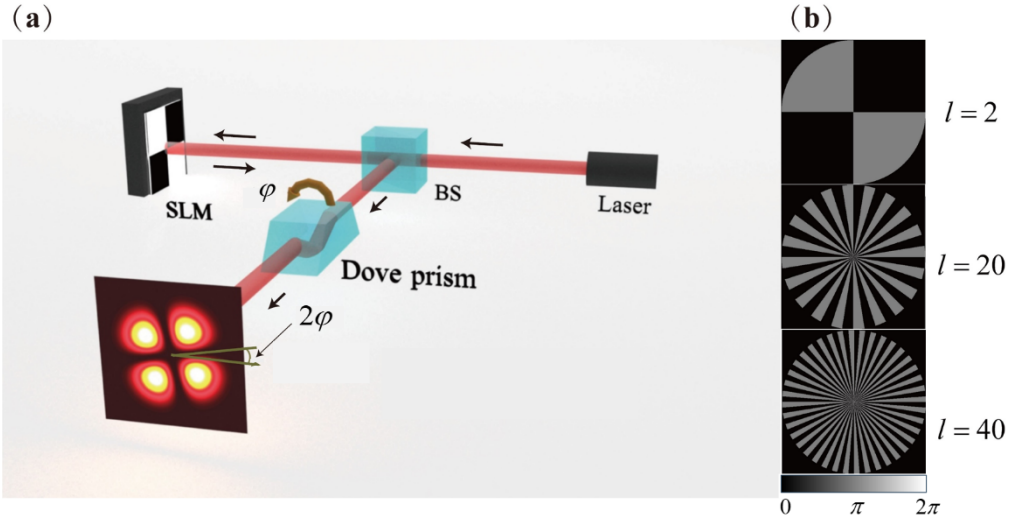

Fig. 2. (a) Experimental configuration. A spatial light modulator (SLM) transforms the fundamental mode of the incident laser beam into l and $-l$ conjugate OAM modes. After passing through the Dove prism, petal-like patterns are recorded by a CCD camera. The pattern here corresponds to $l = 2$. (b) The patterns displayed in the SLM to produce the $+l$ and $-l$ conjugate OAM beams. The black and gray can modulate the optical phase to 0 and π, respectively. The top, middle, and bottom patterns are used to produce petal-like patterns corresponding to $l = 2$, 20, 40, respectively. BS: beam splitter.

areas within the white circle and normalized the total intensity of the selected areas to calculate $S_l(\varphi)$. Without rotating the Dove prism, we can continuously change the direction of the zero azimuthal angle from the maximum intensity of the experimental pattern to simulate the change of φ. According to the theory above, $S_l(\varphi)$ changes with φ periodically. From Eq. (6), we can see that the period, T, is dependent on l of the pattern (i.e., $T = 2\pi/4l$). Figure 3(c) and 3(d) shows $S_l(\varphi)$ with $T = 4.5°$ (or 7.85×10^{-2} radian) for $l = 20$ and 2.25° (or 3.925×10^{-2} radian) for $l = 40$.

Figure 4 shows the dependence of the amplitude of $S_l(\varphi)$ and the slope of $S_l(\varphi)$ for tiny φ on l. In Fig. 4(a), the amplitude of $S_l(\varphi)$ from experimental patterns (black points) decreases with l and are all lower than the theoretical value of $2/\pi$ (red points) from the simulation patterns. We believe that this discrepancy is mainly caused by the gradual decrease of the high-order pattern quality. This indicates that the amplitude of $S_l(\varphi)$ is also related to the quality of the pattern, in addition to the total intensity of the pattern. Thus, when φ is tiny, the slope of $S_l(\varphi)$ in Fig. 4(b) no longer has a linear relationship with l, but still steadily increases with l. It is expected that a higher l produces a higher measured value for certain small rotational angles.

In the experimental system, it is difficult to ensure that the rotational axis, center axis of the Dove prism, and the pattern center overlap perfectly. This usually results in the center of the pattern deviating from the original position during the rotation of the Dove prism. To check this deviation, we rotated the Dove prism from 0° to 0.4° slowly with a step of 0.04° and recorded the patterns for different OAM numbers (i.e., $l = 10$, 20, 30). Figure 5(a) shows the measured $S_l(\varphi)$ as a function of the angular displacement of the Dove prism, φ. The points are calculated from the experimental pattern under rotation of the Dove prism and the lines are calculated from the experimental pattern by changing the zero azimuthal angle. Clearly, the measurement results are in good agreement with the calculated values by changing the zero azimuthal angle. This means the deviation of the pattern center can be neglected when the rotational angle is sufficiently small. It should be noted that the slope of lines increases with l, as was observed in Fig. 4(b).

Optics EXPRESS

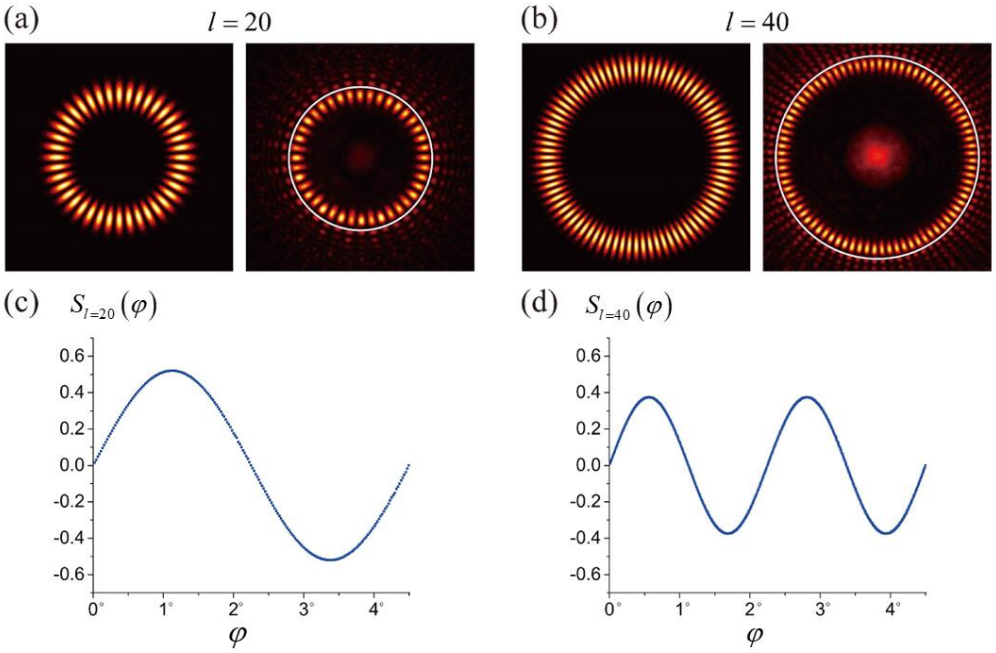

Fig. 3. Petal-like patterns in (a) and (b), and the corresponding $S_l(\varphi)$ in (c) and (d) derived from the experimental pattern. The left side of (a) and (b) are the simulation patterns and the right side are the corresponding experimental patterns. The areas within the white circle of the experimental patterns are normalized to calculate $S_l(\varphi)$. The period of $S_{l=20}(\varphi)$ and $S_{l=40}(\varphi)$ are 4.5° (or 7.85×10^{-2} radian) and 2.25° (or 3.925×10^{-2} radian), respectively.

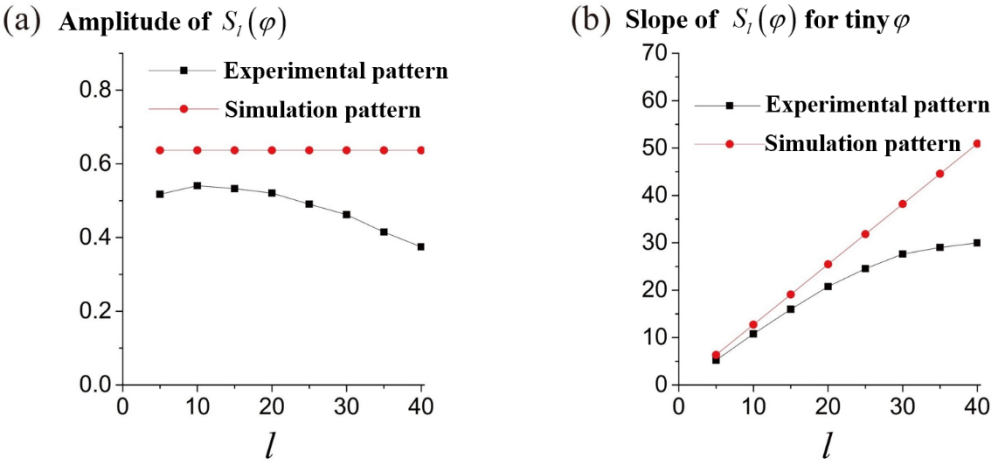

Fig. 4. Amplitude of $S_l(\varphi)$ (a) and slope of $S_l(\varphi)$ for tiny φ (b). The red points are the theoretical values from the simulated patterns and the black points are the values from experimental patterns. The amplitude of $S_l(\varphi)$ from the experimental petals decreases with l as a whole and the values are all lower than the theoretical value of $2/\pi$ from the simulated petals. Thus, the slope of $S_l(\varphi)$ for tiny φ deviates from the theoretical value and no longer has a linear relationship with l.

Optics EXPRESS

Figure 5(b) directly shows that the measurement results are enhanced by l effectively when the Dove prism is rotated by a small angle of 0.04°.

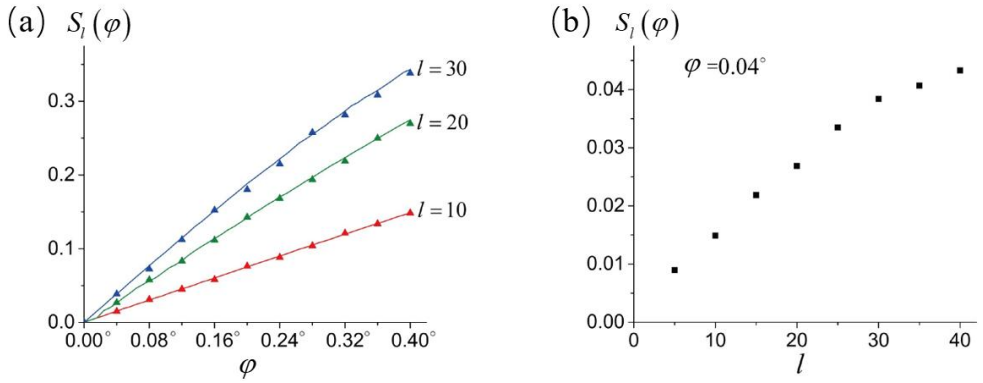

Fig. 5. (a) Measured $S_l(\varphi)$ as a function of φ. The points are calculated from the experimental pattern under rotation of the Dove prism and the lines are calculated from the experimental pattern by changing the zero azimuthal angle for different OAM numbers ($l = 10, 20, 30$). (b) Measurement results when the Dove prism is rotated by an angle of 0.04°.

4. Conclusion

In summary, we have developed a simple experimental system using conjugate orbital angular momentum modes to measure the rotational angle of the Dove prism. Using digital image processing of the rotational pattern, we successfully measured tiny rotational angles. The measurement result was effectively amplified by the OAM. In addition, OAM-enhanced measurement was demonstrated in the presence of defects in both the pattern and light paths. The scheme can be used for sensing and detecting subtle geological changes.

Funding. National Natural Science Foundation of China (61775036, 91851210, 91950206); Research start-up funds of DGUT (211135117); Basic and Applied Basic Research Foundation of Guangdong Province (2021A1515110609, 2023A1515012867).

Disclosures. The authors declare that there are no conflicts of interest related to this article.

Data availability. The data that support the findings of this study are available from the corresponding author upon reasonable request.

References

1. L. Allen, M. W. Beijersbergen, R. J. C. Spreeuw, and J. P. Woerdman, "Orbital angular momentum of light and the transformation of Laguerre-Gaussian laser modes," Phys. Rev. A **45**(11), 8185–8189 (1992).
2. X. Y. Fang, H. R. Ren, and M. Gu, "Orbital angular momentum holography for high-security encryption," Nat. Photonics **14**(2), 102–108 (2020).
3. C. Xu, L. Xiao, J. He, H. Zhang, D. Z. Wei, X. P. Hu, M. Xiao, and Y. Zhang, "Manipulating the radial components of LG pump beam for ultrahigh-dimensional maximally entangled orbital angular momentum states," Opt. Express **30**(7), 11120–11129 (2022).
4. X. Y. Fang, H. R. Ren, K. Y. Li, H. T. Luan, Y. L. Hua, Q. M. Zhang, X. Chen, and M. Gu, "Nanophotonic manipulation of optical angular momentum for high-dimensional information optics," Adv. Opt. Photonics **13**(4), 772–833 (2021).
5. X. Y. Fang, H. J. Wang, H. C. Yang, Z. L. Ye, Y. M. Wang, Y. Zhang, X. P. Hu, S. N. Zhu, and M. Xiao, "Multi-channel nonlinear holography in a two-dimensional nonlinear photonic crystal," Phys. Rev. A **102**(4), 043506 (2020).
6. N. Bozinovic, Y. Yue, Y. Ren, M. Tur, P. Kristenren, H. Huang, A. E. Willner, and S. Ramachandran, "Terabit-Scale Orbital Angular Momentum Mode Division Multiplexing in Fibers," Science **340**(6140), 1545–1548 (2013).
7. J. Wang, J. Y. Yang, I. M. Fazal, N. Ahmed, Y. Yan, H. Huang, Y. Ren, Y. Yue, S. Dolinar, M. Tur, and A. E. Willner, "Terabit free-space data transmission employing orbital angular momentum multiplexing," Nat. Photonics **6**(7), 488–496 (2012).

Optics EXPRESS

8. A. Mair, A. Vaziri, G. Weish, and A. Zeilinger, "Entanglement of the orbital angular momentum states of photons," Nature **412**(6844), 313–316 (2001).
9. A. Nicolas, L. Veissier, L. Giner, E. Giacobino, D. Maxein, and J. Laurat, "A quantum memory for orbital angular momentum photonic qubits," Nat. Photonics **8**(3), 234–238 (2014).
10. N. R. Heckenberg, R. McDuff, C. P. Smith, and A. G. White, "Generation of optical phase singularities by computer generated hologram," Opt. Lett. **17**(3), 221–223 (1992).
11. L. Marrucci, C. Manzo, and D. Paparo, "Optical Spin-to-Orbital Angular Momentum Conversion in Inhomogeneous Anisotropic Media," Phys. Rev. Lett. **96**(16), 163905 (2006).
12. P. Chen, W. Ji, B.-Y. Wei, W. Hu, V. Chigrinov, and Y. Q. Lu, "Generation of arbitrary vector beams with liquid crystal polarization converters and vector-photoaligned q-plates," Appl. Phys. Lett. **107**(24), 241102 (2015).
13. M. W. Beijersbergen, R. P. C. Coerwinkel, M. Kristensen, and J. P. Woerdman, "Helical-wave front laser beams produced with a spiral phaseplate," Opt. Commun. **112**(5-6), 321–327 (1994).
14. R. Zheng, C. Gu, A. Wang, L. Xu, and H. Ming, "An all-fiber laser generating cylindrical vector beam," Opt. Express **18**(10), 10834–10838 (2010).
15. X. Cai, J. Wang, M. J. Strain, B. Johnson-Morris, J. Bo, M. Sorel, J. L. O'Brien, M. G. Thompson, and S. Yu, "Integrated Compact Optical Vortex Beam Emitters," Science **338**(6105), 363–366 (2012).
16. H. Li, D. B. Phillips, X. Wang, Y.-L. D. Ho, L. Chen, X. Zhou, J. Zhu, S. Yu, and X. Cai, "Orbital angular momentum vertical-cavity surface-emitting lasers," Optica **2**(6), 547–552 (2015).
17. M. J. Strain, X. Cai, J. Wang, J. Zhu, D. B. Phillips, L. Chen, M. Lopez-Garcia, J. L. O'Brien, M. G. Thompson, M. Sorel, and S. Yu, "Fast electrical switching of orbital angular momentum modes using ultra-compact integrated vortex emitters," Nat. Commun. **5**(1), 4856 (2014).
18. D. Wei, Y. Cheng, R. Ni, Y. Zhang, X. Hu, S. Zhu, and M. Xiao, "Generating controllable Laguerre-Gaussian laser modes through intracavity spin-orbital angular momentum conversion of light," Phys. Rev. Appl. **11**(1), 014038 (2019).
19. D. Naidoo, F. S. Roux, A. Dudley, I. Litvin, B. Piccirillo, L. Marrucci, and A. Forbes, "Controlled generation of higher-order Poincaré sphere beams from a laser," Nat. Photonics **10**(5), 327–332 (2016).
20. Y. Wu, R. Ni, Z. Xu, Y. Wu, X. Y. Fang, D. Wei, X. P. Hu, Y. Zhang, M. Xiao, and S. N. Zhu, "Tunable third harmonic generation of vortex beams in an optical superlattice," Opt. Express **25**(25), 30820–30826 (2017).
21. X. Y. Fang, G. Yang, D. Wei, D. Wei, R. Ni, W. Ji, Y. Zhang, X. Hu, W. Hu, Y. Q. Lu, S. N. Zhu, and M. Xiao, "Coupled orbital angular momentum conversions in a quasi-periodically poled LiTaO3 crystal," Opt. Lett. **41**(6), 1169–1172 (2016).
22. D. Wei, J. Guo, X. Fang, D. Wei, R. Ni, P. Chen, X. Hu, Y. Zhang, W. Hu, Y. Q. Lu, S. N. Zhu, and M. Xiao, "Multiple generations of high-order orbital angular momentum modes through cascaded third-harmonic generation in a 2D nonlinear photonic crystal," Opt. Express **25**(10), 11556–11563 (2017).
23. D. Z. Wei, Y. Wu, Y. M. Wang, D. M. Liu, Y. Z. Zhu, D. Wei, Y. Zhang, and M. Xiao, "Survival of the orbital angular momentum of light through an extraordinary optical transmission process in the paraxial approximation," Opt. Express **24**(11), 12007 (2016).
24. X. Y. Fang, D. Wei, Y. M. Wang, H. J. Wang, Y. Zhang, X. P. Hu, S. N. Zhu, and M. Xiao, "Conical third-harmonic generation in a hexagonally poled LiTaO3 crystal," Appl. Phys. Lett. **110**(11), 111105 (2017).
25. Y. Zhai, S. Fu, C. Yin, H. Zhou, and C. Gao, "Detection of angular acceleration based on optical rotational Doppler effect," Opt. Express **27**(11), 15518–15527 (2019).
26. M. P. Lavery, F. C. Speirits, S. M. Barnett, and M. J. Padgett, "Detection of a Spinning Object Using Light's Orbital Angular Momentum," Science **341**(6145), 537–540 (2013).
27. Z. J. Zhang, L. Z. Cen, J. D. Zhang, J. Y. Hu, F. Wang, and Y. Zhao, "Rotation velocity detection with orbital angularmomentum light spot completely deviated out of the rotation center," Opt. Express **28**(5), 6859–6867 (2020).
28. Z. J. Zhang, L. Z. Cen, F. Wang, and Y. Zhao, "Tiny velocity measurement using rotating petal-like mode of orbital angular momentum," Opt. Lett. **46**(19), 4805–4808 (2021).
29. W. Zhang, J. Gao, D. Zhang, Y. He, T. Xu, R. Fickler, and L. Chen, "Free-space remote sensing of rotation at photon-counting level," Phys. Rev. Appl. **10**(4), 044014 (2018).
30. H. L. Zhou, D. Z. Fu, J. J. Dong, P. Zhang, D. X. Chen, X. L. Cai, F. L. Li, and X. L. Zhang, "Orbital angular momentum complex spectrum analyzer for vortex light based on the rotational Doppler effect," Light: Sci. Appl. **6**(4), e16251 (2016).
31. D. Wei, J. T. Ma, T. X. Wang, C. Xu, S. N. Zhu, M. Xiao, and Y. Zhang, "Laguerre-Gaussian transform for rotating image processing," Opt. Express **28**(18), 26898–26907 (2020).
32. V. D'Ambrosio, N. Spagnolo, L. Del Re, S. Slussarenko, Y. Li, L. C. Kwek, L. Marrucci, S. P. Walborn, L. Aolita, and F. Sciarrino, "Photonic polarization gears for ultra-sensitive angular measurements," Nat. Commun. **4**(1), 2432 (2013).
33. A. K. Jha, G. S. Agarwal, and R. W. Boyd, "Supersensitive measurement of angular displacements using entangled photons," Phys. Rev. A **83**(5), 053829 (2011).
34. K. Liu, C. Cai, J. Li, L. Ma, H. Sun, and J. Gao, "Squeezing-enhanced rotating-angle measurement beyond the quantum limit," Appl. Phys. Lett. **113**(26), 261103 (2018).

Optics EXPRESS

35. Z. Zhang, T. Qiao, K. Ma, L. Cen, J. Zhang, F. Wang, and Y. Zhao, "Ultra-sensitive and super-resolving angular rotation measurement based on photon orbital angular momentum using parity measurement," Opt. Lett. **41**(16), 3856–3859 (2016).
36. Z. Zhang, T. Qiao, K. Ma, J. Zhang, L. Cen, F. Wang, and Y. Zhao, "Super-resolving angular rotation measurement using binary-outcome homodyne detection," Opt. Express **24**(16), 18477–18485 (2016).
37. S. K. Dacha, W. Zhu, A. Agrawal, K. J. Ritter, and T. E. Murphy, "Nonlinear rotation of spin-orbital coupled states in hollow ring-core fiber," Opt. Express **30**(11), 18481–18495 (2022).
38. O. S. Magaña-Loaiza, M. Mirhosseini, B. Rodenburg, and R. W. Boyd, "Amplification of Angular Rotations Using Weak Measurements," Phys. Rev. Lett. **112**(20), 200401 (2014).
39. S. Xiao, L. Zhang, D. Wei, F. Liu, Y. Zhang, and M. Xiao, "Orbital angular momentum-enhanced measurement of rotation vibration using a Sagnac interferometer," Opt. Express **26**(2), 1997–2005 (2018).
40. N. Gonzalez, G. Molina-Terriza, and J. P. Torres, "How a Dove prism transforms the orbital angular momentum of a light beam," Opt. Express **14**(20), 9093–9102 (2006).